Clinical Cancer Research

PI3K–mTOR Pathway Inhibition Exhibits Efficacy Against High-grade Glioma in Clinically Relevant Mouse Models

Fan Lin[1], Mark C. de Gooijer[1], Diana Hanekamp[1], Gayathri Chandrasekaran[1], Levi C.M. Buil[1], Nishita Thota[1], Rolf W. Sparidans[2], Jos H. Beijnen[2,3], Tom Würdinger[4,5], and Olaf van Tellingen[1]

Abstract

Purpose: The PI3K–AKT–mTOR signaling pathway is frequently activated in glioblastoma and offers several druggable targets. However, clinical efficacy of PI3K/mTOR inhibitors in glioblastoma has not yet been demonstrated. Insufficient drug delivery may limit the efficacy of PI3K/mTOR inhibitors against glioblastoma. The presence of the efflux transporters ABCB1/Abcb1 (P-glycoprotein, MDR1) and ABCG2/Abcg2 (BCRP) at the blood–brain barrier (BBB) restricts the brain penetration of many drugs.

Experimental Design: We used *in vitro* drug transport assays and performed pharmacokinetic/pharmacodynamic studies in wild-type and ABC-transporter knockout mice. The efficacy of PI3K-mTOR inhibition was established using orthotopic allograft and genetically engineered spontaneous glioblastoma mouse models.

Results: The mTOR inhibitors rapamycin and AZD8055 are substrates of ABCB1, whereas the dual PI3K/mTOR inhibitor NVP-BEZ235 and the PI3K inhibitor ZSTK474 are not. Moreover, ABCG2 transports NVP-BEZ235 and AZD8055, but not ZSTK474 or rapamycin. Concordantly, *Abcb1a/b*$^{-/-}$;*Abcg2*$^{-/-}$ mice revealed increased brain penetration of rapamycin (13-fold), AZD8055 (7.7-fold), and NVP-BEZ235 (4.5-fold), but not ZSTK474 relative to WT mice. Importantly, ABC transporters limited rapamycin brain penetration to subtherapeutic levels, while the reduction in NVP-BEZ235 brain penetration did not prevent target inhibition. NVP-BEZ235 and ZSTK474 demonstrated antitumor efficacy with improved survival against U87 orthotopic gliomas, although the effect of ZSTK474 was more pronounced. Finally, ZSTK474 prolonged overall survival in Cre-LoxP conditional transgenic *Pten; p16*^{Ink4a}/*p19*^{Arf};*K-Ras*^{v12};*LucR* mice, mainly by delaying tumor onset.

Conclusions: PI3K/mTOR inhibitors with weak affinities for ABC transporters can achieve target inhibition in brain (tumors), but have modest single-agent efficacy and combinations with (BBB penetrable) inhibitors of other activated pathways may be required. *Clin Cancer Res; 23(5); 1286–98. ©2016 AACR.*

Introduction

Glioblastomas (WHO Grade IV) are the most common primary brain tumors with a median survival of only 15 months, despite intensive treatment including surgery and chemoradiation. Common molecular alterations in glioblastoma include overexpression of EGFR, PDGFR, and cMET, activating mutations in PI3K and EGFR (EGFRvIII) and loss of function of PTEN by deletion or mutations (1, 2). These alterations lead to constitutive activation of PI3K and further downstream effectors such as mTOR, which are crucial for tumor cell growth, proliferation, and survival (3). Preclinical studies suggest that inhibition of this pathway results in either direct inhibition of tumor growth or in sensitizing cells to conventional chemotherapy and radiotherapy (4, 5). Activation of the PI3K–mTOR signaling pathway is a very common event in solid tumors, which triggered the development of numerous small-molecule inhibitors. Although these PI3K inhibitors have been developed mainly for other more common solid tumors, they are now also being tested against glioblastoma (e.g., Clinicaltrials.gov identifiers NCT01339052, NCT00085566, NCT01240460, NCT02430363, NCT01316809) (6). Unfortunately, however, the outcomes of clinical studies with agents that target the PI3K pathway in glioblastoma have been disappointing so far. The prototype mTOR inhibitor rapamycin (sirolimus) and its analogues (so called rapalogs) temsirolimus and everolimus were considered

[1]Department of Bio-Pharmacology/Mouse Cancer Clinic, The Netherlands Cancer Institute (Antoni van Leeuwenhoek Hospital), Amsterdam, the Netherlands. [2]Department of Pharmacy and Pharmacology, The Netherlands Cancer Institute/Slotervaart Hospital, Amsterdam, the Netherlands. [3]Faculty of Science, Department of Pharmaceutical Sciences, Division of Pharmacoepidemiology & Clinical Pharmacology, Utrecht University, Utrecht, the Netherlands. [4]Neuro-oncology Research Group, Departments of Neurosurgery and Pediatric Oncology/Hematology, Cancer Center Amsterdam, VU University Medical Center, Amsterdam, the Netherlands. [5]Molecular Neurogenetics Unit, Departments of Neurology and Radiology, Massachusetts General Hospital, and Neuroscience Program, Harvard Medical School, Boston, Massachusetts.

Note: Supplementary data for this article are available at Clinical Cancer Research Online (http://clincancerres.aacrjournals.org/).

Fan Lin and Mark C. de Gooijer contributed equally to this article.

Current address for F. Lin: Department of Cell Biology, School of basic medical science, Nanjing Medical University, Nanjing, China. Current address for D. Hanekamp, Department of Hematology, VU University medical center, Amsterdam, the Netherlands; current address for G. Chandrasekaran, Cancer Research UK, Cambridge Research Institute, Li Ka Shing Centre, Cambridge, United Kingdom; and current address for N. Thota, Strand Life Sciences, 5th Floor, Kirloskar Business Park, Bellary road, Bengaluru 560024, Karnataka, India.

Corresponding Author: Olaf van Tellingen, AKL Bio-Pharmacology/Mouse Cancer Clinic, Room C1.005, Plesmanlaan 121, Amsterdam 1066CX, the Netherlands. Phone: 31 20 5122792; Fax: 31020512; E-mail: o.v.tellingen@nki.nl

doi: 10.1158/1078-0432.CCR-16-1276

Translational Relevance

Glioblastomas are almost uniformly lethal CNS tumors and better treatments are desperately needed. Although glioblastomas frequently harbor an activated PI3K pathway, clinical trials using PI3K pathway inhibitors conducted thus far have failed. We demonstrate that the blood–brain barrier (BBB) is a major hurdle in glioblastoma treatment, in particular due to ABCB1 and ABCG2 limiting the brain accumulation of many small-molecule drugs. From a panel of PI3K pathway inhibitors, we identified ZSTK474 as a BBB-permeable candidate. At clinically relevant plasma levels, ZSKT474 achieved target inhibition in orthotopic xenograft and transgenic glioma models. Antitumor efficacy was also observed albeit that the effect-size was relatively modest. Our data suggest that BBB-penetrable PI3K inhibitors may play a role in the treatment of glioblastoma, but that single-agent efficacy is modest, hence they may need to be used in combination with agents that inhibit other proliferation signals present in glioblastoma tumor cells.

promising targeted agents for glioblastoma, but a number of phase I and II trials applying them either as monotherapy or in combination with an EGFR inhibitor failed to demonstrate meaningful clinical efficacy in recurrent glioblastoma (7, 8). Possible explanations for this lack of efficacy include a lack of mTORC2 inhibition by rapalogs (9), increased upstream signaling of Akt through negative feedback loops following mTOR inhibition (10, 11), and PTEN status (12). Although these events, which focus on PI3K–mTOR signaling itself, may have contributed to the failures, a frequently underappreciated but critical issue is the presence of the blood–brain barrier (BBB) that may have hampered drug delivery to tumor cells in quantities required to elicit a meaningful pharmacologic response. Especially those glioblastoma cells that escaped surgical resection due to their migration away from the tumor core into adjacent regions of the brain will be shielded by a more intact BBB (13, 14).

It is well known that the intact BBB restricts the brain entry of the majority of xenobiotics by its unique structure (13). In particular, the drug efflux transporters expressed at the BBB play a very important role in limiting the brain penetration of a wide variety of compounds including frequently used chemotherapeutics and novel targeted agents. Two well-established drug efflux transporters, ABCB1 (P-glycoprotein, P-gp, MDR1) and ABCG2 (Breast Cancer Resistance Protein, BCRP), are abundantly expressed in the human and murine BBB and restrict most newly developed kinase inhibitors such as erlotinib, lapatinib, and palbociclib (15–17). As a consequence, the usefulness of such agents in glioblastoma treatment might be attenuated by an inadequate brain penetration.

In the current study, we have compared the affinity for ABCB1 and ABCG2 as well as their impacts on brain penetration of the mTOR inhibitors rapamycin and AZD8055, the PI3K/mTOR inhibitor NVP-BEZ235 and the PI3K inhibitor ZSTK474. All these inhibitors are under investigation for treatment of glioblastoma (18–20). We have used the orthotopic U87 brain tumor model to evaluate the antitumor efficacy of the inhibitors and further investigated ZSTK474, being the PI3K inhibitor with the most favorable brain penetration, in a more clinically relevant transgenic glioblastoma model (21).

Materials and Methods

Reagents

The PI3K inhibitors rapamycin and ZSTK474 were purchased from LC Laboratories. NVP-BEZ235 was purchased from Selleck Chemicals. AZD8055 was purchased from Active Biochem. These compounds were dissolved in DMSO (Sigma-Aldrich) to yield 10 and 4 nmol/L working solutions and were stored at 4°C. Elacridar was kindly provided by GlaxoSmithKline. Zosuquidar (LY335979) was kindly provided by Eli Lilly. Modified Eagle's medium (MEM), Opti-MEM–reduced serum medium, HBSS (Hank's balanced salt solution), L-glutamine, nonessential amino acids, MEM vitamins, penicillin–streptomycin, FCS, trypsin-EDTA, and other reagents for cell culture were purchased from Invitrogen. All other chemicals were purchased from Merck.

Cell lines

LLC and MDCK cell lines used for *in vitro* transport experiments (see below) have been generated in our institute. U87MG human glioma cells have been obtained from ATCC and have been transfected with luciferase in house to obtain clone U87lucB5. All cell lines have been cryopreserved in stocks and aliquots are thawed and used for a maximum period of about 45 days (10–15 passages). Mycoplasma testing and testing for absence of mouse pathogens of the stocks is performed by PCR. The human U87lucB5 line was last authenticated by STR analysis on January 2013 (Identicell).

Animals

Mice were housed and handled according to institutional guidelines complying with Dutch legislation. All experiments with animals were approved by the animal experiment committee of the institute. The animals used for pharmacokinetics studies were female wild-type (WT), *Abcb1a/b*$^{-/-}$, *Abcg2*$^{-/-}$, and *Abcb1a/b*$^{-/-}$;*Abcg2*$^{-/-}$ mice of FVB genetic background, between 9 and 14 weeks of age. *p16*^{Ink4a}*/p19*^{Arf}*;K-Ras*^{v12}*;LucR, Pten;p16*^{Ink4a}*/p19*^{Arf}*;K-Ras*^{v12}*;LucR, p53;p16*^{Ink4a}*/p19*^{Arf}*;K-Ras*^{v12}*;LucR* and *p53;Pten;p16*^{Ink4a}*/p19*^{Arf}*;K-Ras*^{v12}*;LucR* conditional mice for generation of glioblastoma cell lines and efficacy studies were genotyped as described previously (21). The animals were kept in a temperature-controlled environment with a 12-hour dark/ 12-hour light cycle and received a standard diet (AM-II, Hope Farm B.B.) and acidified water *ad libitum*.

In vitro transport experiments

To determine whether rapamycin, AZD8055, NVP-BEZ235, and ZSTK474 are substrates of murine Abcb1a (Mdr1a), human ABCB1 (MDR1), murine Abcg2, and/or human ABCG2, we analyzed the translocation of these compounds in concentration equilibrium transport assays (CETA) as described previously (22). To this end, we used the parental LLC pig-kidney cell line (LLC-PK1) and sublines transduced with murine Abcb1a (LLC-Mdr1a) or human ABCB1 (LLC-MDR1) and the parental Madine Darby Canine Kidney (MDCK) type II cell line (MDCKII-parental) and murine Abcg2 (MDCKII-Bcrp1) or human ABCG2–transduced sublines (MDCKII-BCRP). Cells were seeded on Transwell microporous polycarbonate membrane filters (3.0-μm pore size, 24-mm diameter; Costar Corning) at a density of 2×10^6 cells

per well in 2-mL MEM. When confluency was reached, the transport experiment was started by replacing the drug-free medium with Opti-MEM medium containing 0.5 μmol/L rapamycin, or MEM containing 1 μmol/L AZD8055, 0.5 μmol/L ZSTK474, or 0.5 μmol/L NVP-BEZ235. Zosuquidar (5 μmol/L) or Elacridar (5 μmol/L) was added when appropriate to inhibit either Abcb1 alone or both Abcb1 and Abcg2, respectively. [^{14}C]-inulin (approximately 1.6×10^6 DPM/mL) was added to check the integrity of the membrane. Samples of 50 μL were taken at 30, 120, 180, and 240 minutes and used for drug analysis.

Colony formation assays

U87 human glioma cells were seeded in 24-well plates and exposed to various concentrations of NVP-BEZ235 or ZSTK474. Upon reaching confluency in the control wells, all cells were fixed and stained using a glutaraldehyde (6% v/v; Sigma) and crystal violet (0.5% w/v; Sigma) solution. Plates were imaged using a Chemi-Doc MP system (Bio-Rad) and well confluency was measured using the ImageJ plugin ColonyArea as described elsewhere (23). Curves were plotted, fitted with a log(inhibitor) versus response - Variable slope (four parameters) curve and IC_{50}s were determined using GraphPad Prism 5.01 (GraphPad Software, Inc.).

Drug formulations

For pharmacokinetic studies, rapamycin was first dissolved in 100% ethanol and further diluted in HBSS to yield a solution of 0.05 mg/mL. AZD8055 was dissolved in DMSO at a concentration of 10 mg/mL. For orally administration, ZSTK474 was mixed with water and sonicated, suspended in a mixture of hydroxypropyl methylcellulose (4%, v/v) and Tween 80 (polysorbate 80; 0.75%, v/v) to yield a drug suspension of 20 mg/mL. For intravenous administration, ZSTK474 was dissolved in DMSO to yield a solution of 10 mg/mL. NVP-BEZ235 was dissolved in DMSO to yield a solution of 5 mg/mL and further mixed with PEG400 to yield a solution of 1 mg/mL.

Plasma and brain pharmacokinetics

Rapamycin (1.5 mg/kg, i.p.), AZD8055 (10 mg/kg, i.v.), NVP-BEZ235 (10 mg/kg, orally), and ZSTK474 (10 mg/kg, i.v.; 200 mg/kg orally) were administered to WT and *Abcb1a/b;Abcg2*$^{-/-}$ mice and/or *Abcb1a/b*$^{-/-}$ and *Abcg2*$^{-/-}$ mice. Elacridar, prepared as described previously (24), was given orally at a dose of 100 mg/kg 15 minutes prior to rapamycin. Blood sampling was performed either by collecting tail vein blood or by cardiac puncture at different time points. Brains were dissected after mice were sacrificed and were homogenized in 3 mL 1% (w/v) BSA. Both plasma and brain homogenates were stored at −20°C until analysis.

Drug analytic method

Rapamycin (MRM 936.6/409.2) was measured using LC-ESI-MS/MS with tacrolimus (826.5/616.2) as internal standard and protein precipitation with methanol for sample pretreatment. Samples of 5 μL were injected onto an Atlantis dC18 column (Waters) coupled with a Polaris 3 C18-A precolumn (Varian). The gradient elution of methanol ranged from 65% to 100% (v/v) in 1% (v/v) formic acid. Spray voltage was set to 3,900 V, capillary temperature to a 400°C and argon collision pressure to 2.0 mTorr. Collision energies were at 54 and 36 V, respectively.

AZD8055 (MRM 466.4/450.3) was measured using LC-ESI-MS/MS with buparlisib (411.3/367.2) as internal standard and ethyl acetate extraction as sample pretreatment. Samples of 50 μL were injected onto an Agilent C18 column (Agilent) coupled with a Phenomenex analytic securityguard C18 precolumn (Phenomenex). The gradient elution of methanol ranged from 65% to 100% (v/v) in 0.1% (v/v) formic acid. Declustering potential was 100 V and collision energy 59 eV.

For quantification of ZSTK474 in plasma and brain samples, a reversed-phase high-performance liquid chromatographic (HPLC) assay with fluorometric detection was used. Following tert-butyl methyl ether extraction, ZSTK474 and its internal standard NVP-BEZ235 were chromatographically separated using XBridge BEH130 C18 column (Waters) by isocratic elution with a mobile phase which consisted of acetonitrile, and 0.1% triethylamine adjusted with hydrochloric acid to pH 9.5 (50:50, v/v). Fluorescence detection was used with excitation and emission wavelengths of 240 and 425 nm, respectively. NVP-BEZ235 concentration in biological samples was measured using an HPLC assay as described previously (25).

Stereotactic intracranial injections and bioluminescence imaging

The detailed procedures of stereotactic intracranial injection and bioluminescence imaging have been described previously (26). In short, FVB nude mice or *p16*^{Ink4a}*/p19*^{Arf}*;K-Ras*^{v12}*;LucR*, *Pten;p16*^{Ink4a}*/p19*^{Arf}*;K-Ras*^{v12}*;LucR*, *p53;p16*^{Ink4a}*/p19*^{Arf}*;K-Ras*^{v12}*;LucR* or *p53;Pten;p16*^{Ink4a}*/p19*^{Arf}*;K-Ras*^{v12}*;LucR* mice were anaesthetized and placed in a stereotactic frame, 10^5 U87-luc cells or CMV-Cre lentivirus suspension in 2 μL was injected 2 mm lateral and 1 mm anterior to the bregma, 3 mm below the skull cap. After the initial tumor load was established, tumor development was monitored by bioluminescence using the IVIS 200 Imaging system (Xenogen Corporation). Mice were sacrificed when clear neurologic symptoms occurred or weight loss ($\geq$ 20%) was observed. Brain tissue was fixed in an ethanol–glacial acetic acid mixture containing 4% formaldehyde (EAF), embedded in paraffin, and cut into coronal slices of 4 μm. Sections were H&E stained for verification of tumor growth.

Glioma mouse model intervention study

For the U87 xenograft model drug intervention study, animals were stratified on the basis of bioluminescence signal at day 12 after tumor cell injection into three groups receiving daily vehicle control solution (orally 200 μL saline per mouse), NVP-BEZ235 (orally 10 mg/kg), or ZSTK474 (orally 200 mg/kg), respectively, until the day of sacrifice. For the spontaneous glioblastoma model drug intervention study, animals received a dose of 200 mg/kg every day of ZSTK474, starting 3 days after lentiviral injection until the day of sacrifice.

Histology and IHC

Brain tissue was fixed in 4% formaldehyde, paraffin-embedded, and cut into 4-μm coronal sections that were stained with H&E and for pAKT (D9E), pERK (D13.14.4E), and p4EBP1 (236B4; Cell Signaling Technology).

Pharmacokinetic calculations and statistical analysis

As previously described, the general linear model repeated-measures procedure was used to determine whether the basolateral-to-apical differences of the drugs levels were significantly

increased by the factor of time and at which time point(s) these differences became significant (27). For *in vivo* pharmacokinetic experiments, pharmacokinetic parameters were calculated using an add-in program for Microsoft Excel PKSolver (28). To determine the differences of brain and plasma concentrations among multiple strains, one-way ANOVA with Bonferroni *post hoc* test was performed. Differences were considered statistically significant when $P < 0.05$. For *in vivo* efficacy studies, survival fractions were calculated using Kaplan–Meier method using GraphPad Prism 5.01 (GraphPad Software). The log-rank test was used to compare survival of groups.

Results

Abcb1 severely impairs the brain penetration of rapamycin

To determine substrate affinity of rapamycin for Abcb1a (Mdr1a) and Abcg2 (Bcrp1), a concentration equilibrium transport assay (CETA) was performed using murine Mdr1a- and Bcrp1-transduced cells and their parental cell lines as described previously (29). Rapamycin was significantly translocated from the basolateral to apical (b-to-a) compartment by LLC-PK1 cells (Fig. 1A). Endogenously expressed porcine Abcb1 was responsible for this translocation, as translocation

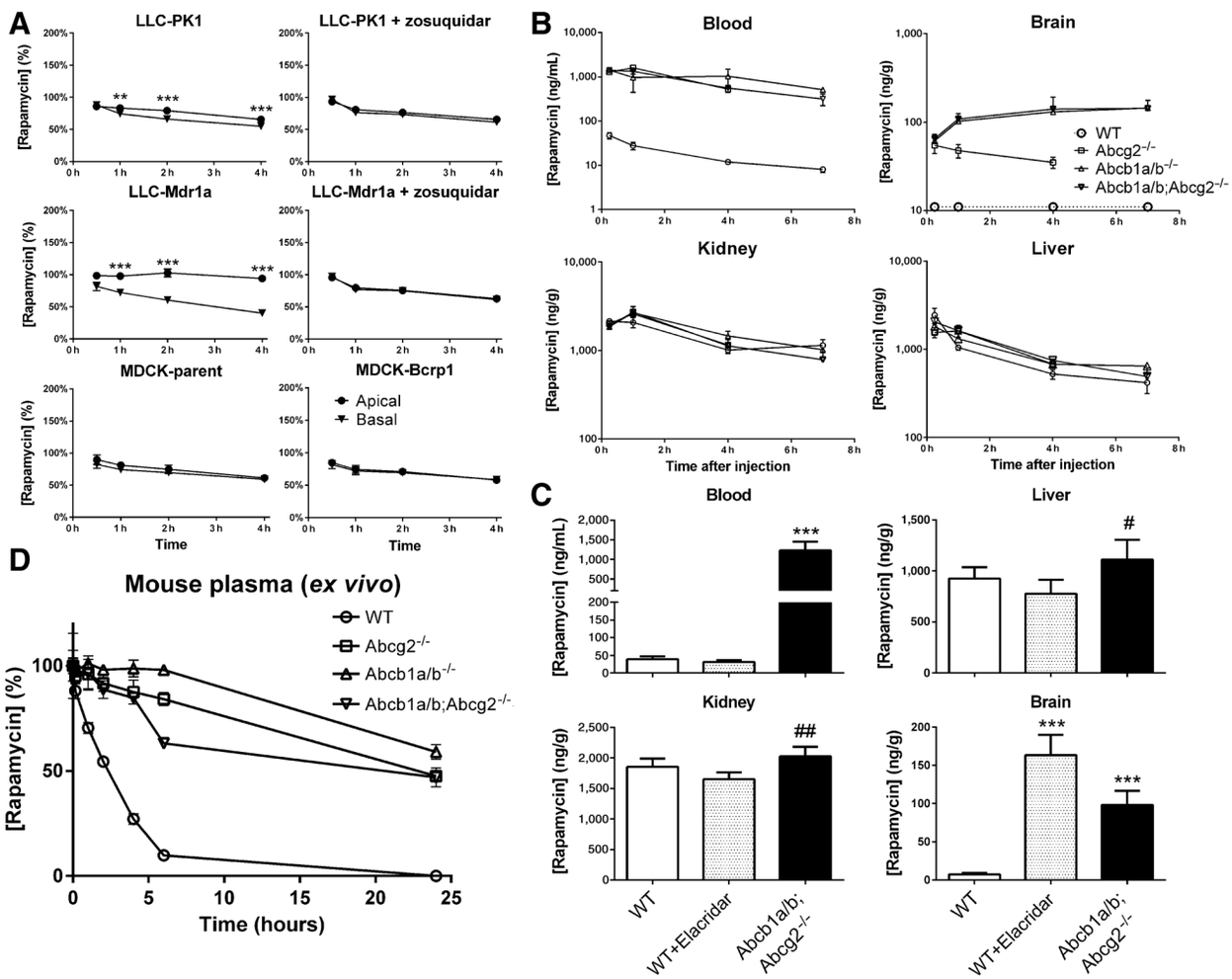

Figure 1.

In vitro transport, *in vivo* pharmacokinetics, and *ex vivo* stability of rapamycin. **A,** Concentration equilibrium transport assays (CETA) for rapamycin using Mdr1a- and Bcrp1-overexpressing cell lines and their parental counterparts (LLC-PK1 and MDCK-parent, respectively). In CETA, the same drug solution is added to both compartments and this concentration is designated 100%. Zosuquidar (5 μmol/L) was used to specifically inhibit P-gp–mediated transport. Data are means ± SD; $n = 6$; **, $P < 0.01$; ***, $P < 0.001$. **B,** Rapamycin levels in blood, brain, kidney, and liver of WT, *Abcb1a/b*$^{-/-}$, *Abcg2*$^{-/-}$, and *Abcb1a/b;Abcg2*$^{-/-}$ mice following intraperitoneal administration of 1.5 mg/kg rapamycin. Data are means ± SD; $n = 3$-4. **C,** Effect of elacridar on rapamycin levels in blood, brain, kidney, and liver of WT mice and *Abcb1a/b;Abcg2*$^{-/-}$ mice receiving rapamycin alone. Elacridar (100 mg/kg) was orally administered to WT mice 15 minutes prior to rapamycin (1.5 mg/kg, i.p.) administration and samples were taken at 1 hour after rapamycin administration. Data are means ± SD; $n = 5$; ***, $P < 0.001$, compared with WT mice without elacridar; #, $P < 0.05$; ##, $P < 0.01$, compared with WT mice with elacridar. **D,** *Ex vivo* stability of rapamycin at 37°C in plasma of WT, *Abcb1a/b*$^{-/-}$, *Abcg2*$^{-/-}$, and *Abcb1a/b*$^{-/-}$*;Abcg2*$^{-/-}$ mice. Data are means ± SD; $n = 3$.

was abrogated when the specific Abcb1 inhibitor zosuquidar was added. Rapamycin b-to-a translocation in Abcb1a-overexpressing LLC-Mdr1a cells was more pronounced than in LLC-PK1 cells and was also completely inhibited by zosuquidar, showing that rapamycin is a good Abcb1 substrate. In contrast, rapamycin is not a substrate of Abcg2, as no b-to-a translocation was observed in Bcrp1-overexpressing MDCK cells (MDCK-Bcrp1).

Next, we assessed the impact of Abcb1 and Abcg2 on rapamycin pharmacokinetics using WT, *Abcb1a/b*$^{-/-}$, *Abcg2*$^{-/-}$, and *Abcb1a/b;Abcg2*$^{-/-}$ mice. Surprisingly, administration of 1.5 mg/kg rapamycin orally resulted in 35- to 52-fold higher AUC_{blood} values in all different knockout mice compared with WT mice (Fig. 1B). However, no differences in rapamycin levels between WT and knockout mice were found in well-perfused organs such as the kidney or liver, where drug levels are usually well equilibrated with systemic blood levels. In the brain, Abcb1 is clearly a dominant factor because the brain AUC of rapamycin in *Abcb1a/b*$^{-/-}$ mice was at least 10-fold higher than in WT mice. The levels in brain samples of WT mice were below the lower limit of quantification (LLQ) of the assay (10 ng/g), whereas the levels in brain samples from Abcg2$^{-/-}$ mice taken at the earlier time points were above the LLQ (Fig. 1B), This is most likely due to the presence of some remnant blood in the homogenized brain tissue and the much higher blood levels of rapamycin in this strain. No significant difference was found between the *Abcb1a/b*$^{-/-}$ and *Abcb1a/b;Abcg2*$^{-/-}$ mice, suggesting Abcg2 is not involved in restricting rapamycin from the brain.

To further investigate whether Abcb1- and/or Abcg2-mediated transport is responsible for the differences of plasma and brain levels between WT and knockout mice, the dual Abcb1 and Abcg2 inhibitor elacridar was coadministrated to WT mice 30 minutes prior to intraperitoneal administration of rapamycin. Moreover, the LC/MS-MS assay was adapted to improve the LLQ and allow accurate quantification in brain samples of WT mice. Interestingly, elacridar enhanced the brain concentration of rapamycin in WT mice by about 23-fold, but did not cause any alteration of rapamycin levels in blood and kidney, indicating that Abcb1a/b and Abcg2 are not responsible for the differences observed in blood of knockout mice (Fig. 1C). Together, these results demonstrate that Abcb1 at the BBB profoundly impairs the brain penetration of rapamycin.

It has previously been reported that rapamycin is unstable in plasma and whole blood of human, rabbit, and rat (30). In contrast to plasma, rapamycin levels in the kidney and liver in our study were not different between WT and knockout mice. Therefore, we tested the stability of rapamycin in murine plasma *ex vivo* and indeed found a much more rapid degradation in plasma of WT compared with ABC-transporter knockout mice. After 6-hour incubation of rapamycin with freshly collected plasma from mice of different knockout strains, we observed that about 85% of the added rapamycin was recovered in plasma of *Abcb1a/b*$^{-/-}$, *Abcg2*$^{-/-}$ and *Abcb1a/b;Abcg2*$^{-/-}$ mice, but about 10% in plasma of WT mice (Fig. 1D). Recent work with rapamycin's analogue everolimus has demonstrated that carboxyl esterase 1c is more abundantly present in ABC-transporter knockout mice and responsible for enhanced stability in plasma (31). It is very likely that the higher blood level of rapamycin in knockout mice is similarly caused by avid binding of rapamycin to a serum factor, possibly Ces1c, which is more abundantly present in the plasma of knockout mice. Because of this avid binding, only a small fraction of rapamycin is available for degradation and for tissue distribution.

Abcb1 and Abcg2 restrict AZD8055 brain penetration

AZD8055 was transported *in vitro* by human and murine MDR1/Mdr1a and BCRP/Bcrp1 (Fig. 2A). Basolateral-to-apical translocation was observed in CETAs with Abcb1a, ABCB1, Abcg2, and ABCG2-overexpressing cell lines, but not parental control lines. Inhibition with zosuquidar or elacridar diminished translocation in all cases and validated AZD8055 transport by MDR1/Mdr1a and BCRP, although Bcrp1-mediated translocation was not completely inhibited by elacridar, indicative of very efficient transport.

Compared with WT mice, the AZD8055 brain concentrations were 3.7- ($P < 0.01$) and 7.7-fold ($P < 0.0001$) higher in *Abcb1a/b*$^{-/-}$ and *Abcb1a/b;Abcg2*$^{-/-}$ mice, respectively (Fig. 2B), whereas the levels in liver and kidney were not different (not shown). Interestingly, a similar plasma retention effect in ABC-transporter knockout mice was found as observed for rapamycin albeit that the effect size was much more modest. Consequently, the brain–plasma ratios do not correctly reflect AZD8055 brain penetration in WT mice versus the knockout mice. However, the increased ratio in *Abcb1a/b;Abcg2*$^{-/-}$ mice in comparison with each of the single knockout strains clearly demonstrates that both Abcb1a/b and Abcg2 restrict the BBB penetration of AZD8055.

NVP-BEZ235 is a substrate of Abcg2 but its brain penetration is mainly limited by Abcb1

Using *in vitro* CETAs, neither LLC-PK1, LLC-Mdr1a, nor LLC-MDR1 cells displayed significant b-to-a translocation of NVP-BEZ235, suggesting that NVP-BEZ235 is not transported by murine or human Abcb1/ABCB1 (Fig. 3A). In contrast, NVP-BEZ235 was significantly translocated by MDCK-Bcrp1 cells, but not MDCK-parent or MDCK-BCRP cells, and this translocation was inhibited by elacridar, indicating that NVP-BEZ235 is transported by murine Abcg2, but not human ABCG2.

The roles of Abcb1 and Abcg2 in limiting the brain penetration of NVP-BEZ235 were investigated using WT and *Abcb1a/b;Abcg2*$^{-/-}$ mice. We administered NVP-BEZ235 orally at a dose of 10 mg/kg. As shown in Fig. 3B, both plasma and brain levels of NVP-BEZ235 were significantly higher in *Abcb1a/b;Abcg2*$^{-/-}$ mice than those in WT mice at multiple time points. Moreover, the brain-to-plasma ratio of *Abcb1a/b;Abcg2*$^{-/-}$ mice was 2.0- ($P < 0.01$) and 1.6-fold ($P < 0.01$) higher than that of WT mice at 1 and 4 hours, respectively. These data suggest that the higher brain level of NVP-BEZ235 was due to the absence of active brain efflux mediated by Abcb1 and Abcg2 and not only a consequence of higher plasma levels in *Abcb1a/b;Abcg2*$^{-/-}$ mice. Interestingly, in contrast to the results obtained from the CETAs, pharmacokinetic experiments with single transporter knockouts showed the brain penetration of NVP-BEZ235 to be predominantly impaired by Abcb1a/b (Fig. 3C). The brain concentration and brain-to-plasma ratio in WT mice were 3.6- ($P < 0.05$) and 1.7-fold ($P < 0.01$) lower than those of *Abcb1a/b*$^{-/-}$ mice and 4.5- ($P < 0.01$) and 2.0-fold ($P < 0.001$) lower than those of *Abcb1a/b;Abcg2*$^{-/-}$ mice, but similar to *Abcg2*$^{-/-}$ mice. Similar to AZD8055, and to a lesser extent to rapamycin, the plasma levels in all knockout strains were higher than in WT mice.

To assess the pharmacodynamic implications of the impaired brain penetration of both NVP-BEZ235 and rapamycin, target

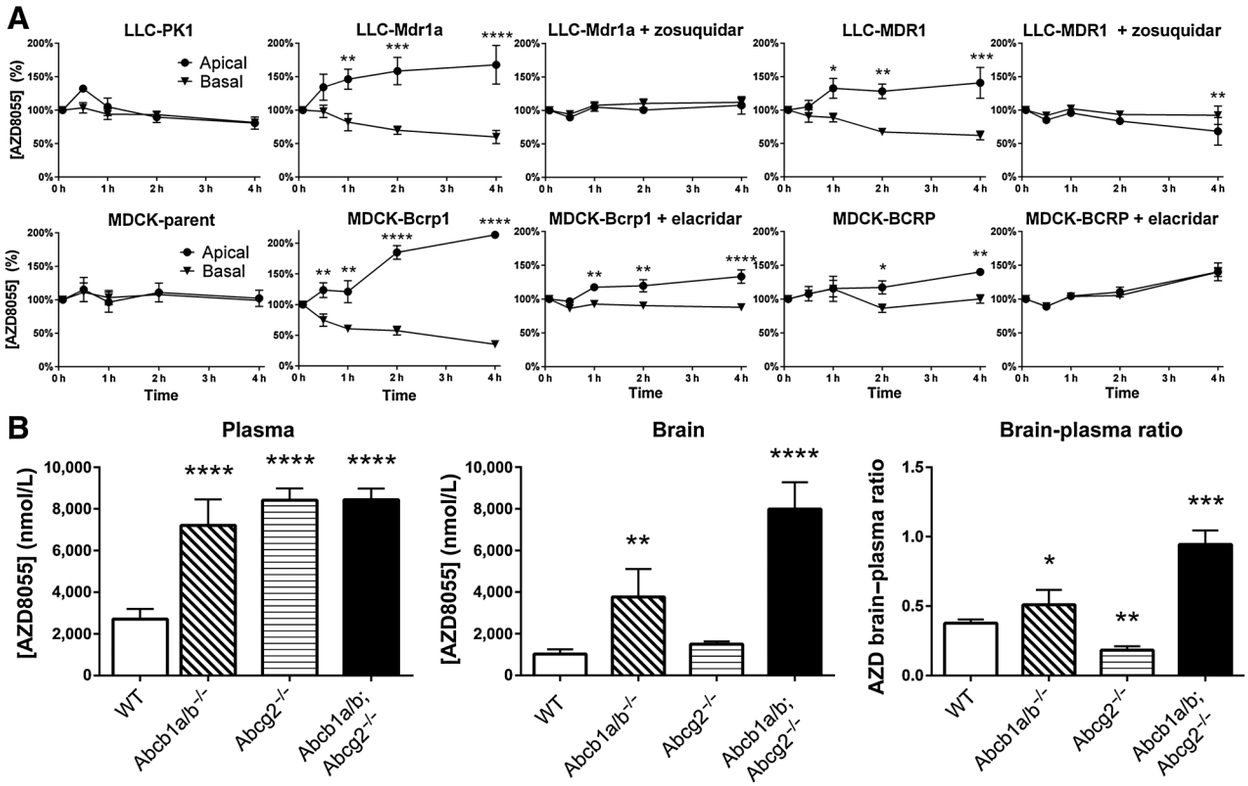

Figure 2.

In vitro transport and *in vivo* pharmacokinetics of AZD8055. **A,** Concentration equilibrium transport assays for AZD8055 using Mdr1a/MDR1 and Bcrp1/BCRP–overexpressing cell lines and their parental counterparts (LLC-PK1 and MDCK-parent, respectively). Zosuquidar or elacridar (5 μmol/L) was used to specifically inhibit P-gp or P-gp/BCRP–mediated transport, respectively. Data are means ± SD; $n = 6$; *, $P < 0.05$; **, $P < 0.01$; ***, $P < 0.001$; ****, $P < 0.0001$. **B,** AZD8055 plasma concentration, brain concentration, and brain–plasma ratios in WT, *Abcb1a/b*$^{-/-}$, *Abcg2*$^{-/-}$, and *Abcb1a/b;Abcg2*$^{-/-}$ mice 1 hour after 10 mg/kg, i.v. administration. Data are means ± SD; $n = 4$; *, $P < 0.05$; **, $P < 0.01$; ***, $P < 0.001$; ****, $P < 0.0001$.

engagement was compared between healthy brain tissue of WT and *Abcb1a/b;Abcg2*$^{-/-}$ mice. At clinically achievable plasma exposures, both rapamycin and NVP-BEZ235 were not very efficient in reducing the phosphorylation levels of the downstream mTOR target pS6 in WT mice relative to control. In contrast, both compounds did inhibit pS6 phosphorylation in *Abcb1a/b;Abcg2*$^{-/-}$ mice, with NVP-BEZ235 also reducing the phospho-AKT^{S473} levels (Fig. 3D). In summary, these data show that Abcb1a/b at the BBB can impair rapamycin and NVP-BEZ235 brain penetration, resulting in hampered intracranial target engagement and thus likely restricting therapeutic efficacy.

ZSTK474 brain penetration is not restricted by Abcb1 and Abcg2

No significant directional translocation of ZSTK474 was found *in vitro*, although a minor ZSTK474 concentration difference was observed at 4 hours in the MDCK-Bcrp1 CETA (Fig. 4A). These data indicate that ZSTK-474 is not transported by Abcb1/ABCB1 or Abcg2/ABCG2.

As the ABC-transporter affinities of a drug can be underestimated when using *in vitro* CETA (see for example NVP-BEZ235), we further investigated the roles of Abcb1 and Abcg2 on brain and plasma pharmacokinetics by oral administration of 200 mg/kg of ZSTK474 to WT and *Abcb1a/b;Abcg2*$^{-/-}$ mice. ZSTK474 plasma and brain concentrations as well as brain-to-plasma ratio were similar in WT and *Abcb1a/b;Abcg2*$^{-/-}$ mice (Fig. 4B). Moreover, oral administration of ZSTK474 greatly diminished PI3K pathway signaling in brain of both WT and *Abcb1a/b;Abcg2*$^{-/-}$ mice, suggesting that sufficient ZSTK474 was delivered to inhibit its target in the brain even in presence of Abcb1 and Abcg2 (Fig. 4C).

We repeated the brain penetration study with ZSTK474 at a lower intravenous dose (10 mg/kg). Again, we did not find any significant difference in plasma, brain concentration, or brain-to-plasma ratio between WT and *Abcb1a/b;Abcg2*$^{-/-}$ mice, confirming that neither systemic clearance nor brain penetration are limited by Abcb1 and Abcg2 (Fig. 4D).

Brain-penetrable PI3K/mTOR inhibitors display efficacy against orthotopic U87

The antitumor efficacy of the brain penetrable inhibitors NVP-BEZ235 ($IC_{50} = 17$ nmol/L; Fig. 5A) and ZSTK474 ($IC_{50} = 630$ nmol/L; Fig 5B) was investigated in the U87 orthotopic xenograft model. Daily administration of NVP-BEZ235 (10 mg/kg orally) and ZSTK474 (200 mg/kg orally) profoundly reduced tumor growth compared with control (Fig. 5C), without diminishing body weight (data not shown). Possibly in line with the slightly lower effect on tumor growth inhibition, NVP-BEZ235–treated mice survival did not significantly differ from control mice, whereas ZSTK474 demonstrated a markedly longer survival than control (median survival 25.0 vs. 17.5 days; $P = 0.0019$).

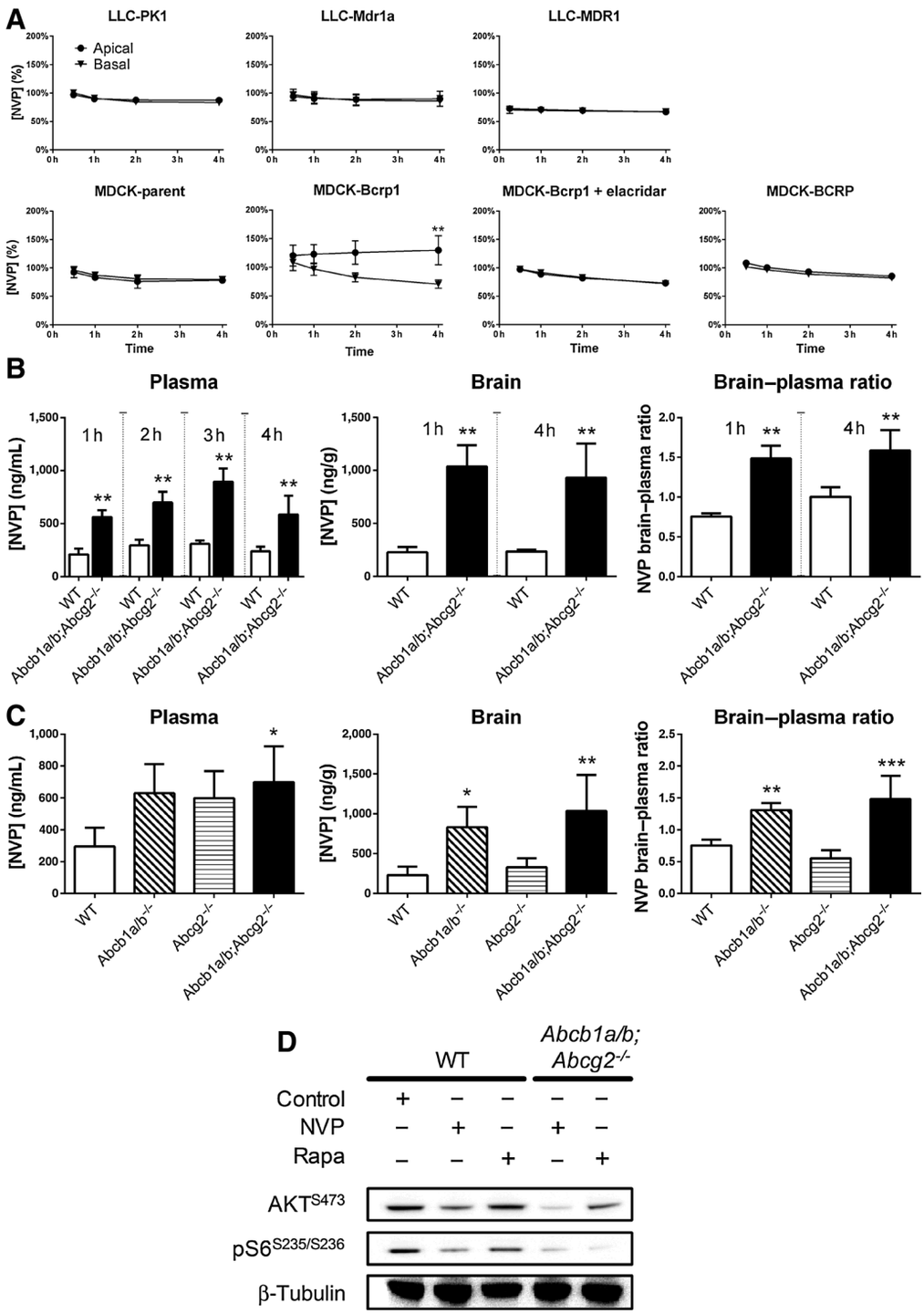

Figure 3.

In vitro transport, *in vivo* pharmacokinetics, and target inhibition of NVP-BEZ235. **A,** Concentration equilibrium transport assays for NVP-BEZ235 using Mdr1a/MDR1 and Bcrp1/BCRP–overexpressing cell lines and their parental counterparts (LLC-PK1 and MDCK-parent, respectively). Elacridar (5 μmol/L) was used to specifically inhibit P-gp/BCRP–mediated transport, respectively. Data are means ± SD; $n = 6$; **, $P < 0.01$. **B,** NVP-BEZ235 plasma concentration, brain concentration, and brain–plasma ratios in WT and *Abcb1a/b;Abcg2*$^{-/-}$ mice 1 and 4 hours after 10 mg/k oral administration. Data are means ± SEM; $n = 5$; **, $P < 0.01$. **C,** NVP-BEZ235 plasma concentration, brain concentration, and brain–plasma ratios in WT, *Abcb1a/b*$^{-/-}$, *Abcg2*$^{-/-}$, and *Abcb1a/b;Abcg2*$^{-/-}$ mice 1 hour after 10 mg/kg oral administration. Data are means ± SD; $n = 4$; *, $P < 0.05$; **, $P < 0.01$; ***, $P < 0.001$. **D,** Western blotting of PI3K–mTOR signaling in brains of healthy WT and *Abcb1a/b; Abcg2*$^{-/-}$ mice that received 1.5 mg/kg rapamycin (Rapa) i.p., 10 mg/kg NVP-BEZ235 (NVP) orally, or no treatment. See Supplementary Methods for details on antibodies.

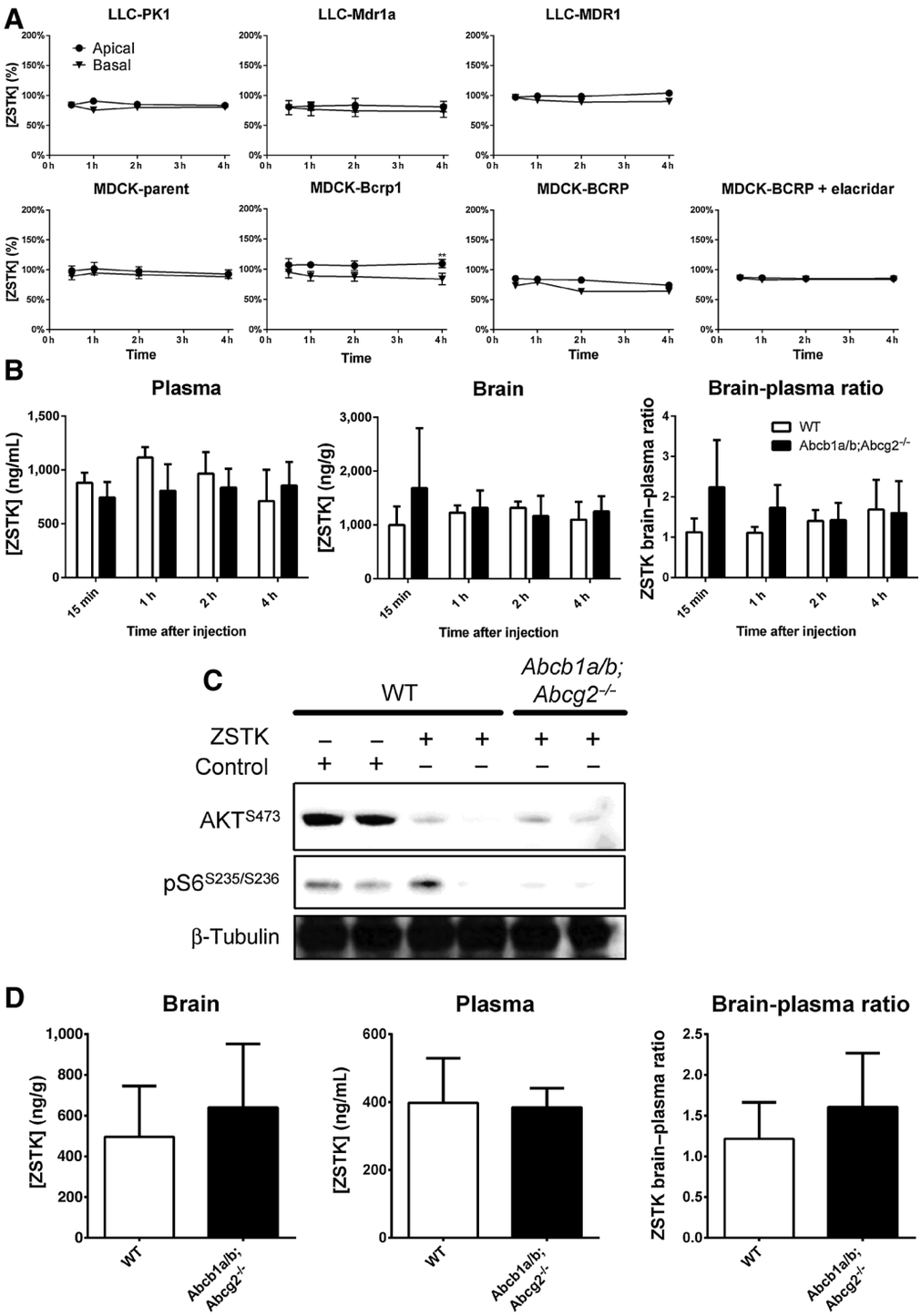

Figure 4.

In vitro transport, *in vivo* pharmacokinetics, and target inhibition of ZSTK474. **A,** Concentration equilibrium transport assays for ZSTK474 using Mdr1a/MDR1 and Bcrp1/BCRP–overexpressing cell lines and their parental counterparts (LLC-PK1 and MDCK-parent, respectively). Elacridar (5 μmol/L) was used to specifically inhibit P-gp/BCRP–mediated transport, respectively. Data are means ± SD; $n = 6$; **, $P < 0.01$. **B,** ZSTK474 plasma concentration, brain concentration, and brain–plasma ratios in WT and *Abcb1a/b;Abcg2*$^{-/-}$ mice at various time points after 200 mg/kg oral administration. Data are means ± SD; $n = 5$. **C,** Western blotting of PI3K–mTOR signaling in brains of healthy WT and *Abcb1a/b;Abcg2*$^{-/-}$ mice that received 200 mg/kg ZSTK474 (ZSTK) orally, or no treatment. Data are shown for two independent animals per group. **D,** ZSTK474 plasma concentration, brain concentration, and brain–plasma ratios in WT and *Abcb1a/b;Abcg2*$^{-/-}$ mice 1 hour following 10 mg/kg i.v. administration. Data are means ± SD; $n = 7$–9.

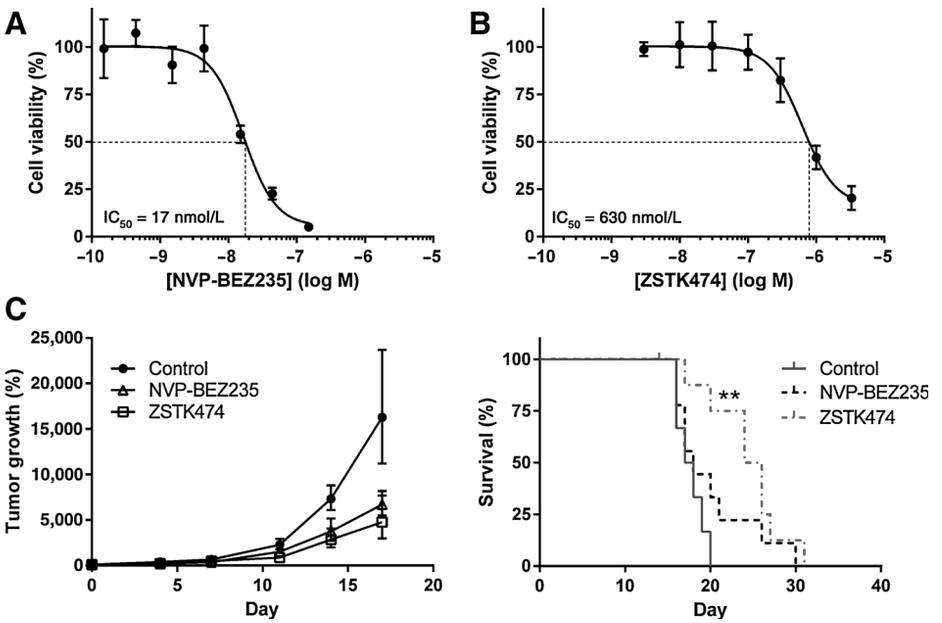

Figure 5.
In vitro and *in vivo* efficacy of NVP-BEZ235 and ZSTK474 against the U87 orthotopic xenograft model. Colony formation assay to establish the IC_{50} of NVP-BEZ235 (17 nmol/L; **A**) and ZSTK474 (630 nmol/L; **B**) against U87 cells *in vitro*. Data are means ± SD; $n = 6$. **C,** Efficacy of NVP-BEZ235 and ZSTK474 against the U87 orthotopic xenograft mouse model. Three groups of WT mice bearing orthotopic U87 tumors received vehicle control, 200 mg/kg/every day ZSTK474, or 10 mg/kg/every day NVP-BEZ235, respectively. Data are means ± SD; $n = 6$, 9, and 9 for Control, ZSTK474, and NVP-BEZ235 groups, respectively; **, $P < 0.01$.

Inhibiting the PI3K signaling in glioblastoma cells and spontaneous glioblastoma models

The antiproliferative activities of NVP-BEZ235 and ZSTK474 were assessed *in vitro* using glioblastoma cells derived from spontaneous transgenic high-grade glioma mouse models as described previously (ref. 21;Supplementary Methods). These cells harbor a combination of genetic deletions that are common in human glioblastoma, including $p16^{Ink4a}/p19^{Arf}$, P53, and/or Pten together with an activated Ras–MAPK pathway. Both agents showed a dose-dependent growth-inhibitory activity in line with target inhibition against all glioblastoma cell lines, with NVP-BEZ235 being approximately 10-fold more potent than ZSTK474 (Supplementary Fig. S1). Pten deficiency did not render these glioblastoma cell lines sensitive to PI3K pathway inhibition, as no clear difference in response was found between the different genotypes.

Traditional xenograft models such as the U87 model fail to recapitulate many important features of human glioma, including BBB integrity. We previously established spontaneous high-grade gliomas models using conditional mice of different genetic backgrounds: *viz.* $p16^{Ink4a}/p19^{Arf}$;$K\text{-}Ras^{v12}$;*LucR*, *Pten*;$p16^{Ink4a}/p19^{Arf}$;$K\text{-}Ras^{v12}$;*LucR*, *p53*;$p16^{Ink4a}/p19^{Arf}$;$K\text{-}Ras^{v12}$;*LucR* and *p53;Pten*;$p16^{Ink4a}/p19^{Arf}$;$K\text{-}Ras^{v12}$;*LucR* (21). All of these mice spontaneously develop grade III or IV gliomas after intracranial CMV-Cre lentivirus injection that exhibit many histopathologic and biological features of high-grade gliomas. In comparison, our glioblastoma models that are deficient for PTEN proliferated much more rapidly *in vivo* than PTEN-proficient $p16^{Ink4a}/p19^{Arf}$;$K\text{-}Ras^{v12}$ tumors (Fig. 6A). As a result, $p16^{Ink4a}/p19^{Arf}$;$K\text{-}Ras^{v12}$ mice that develop gliomas survived significantly longer than *Pten*;$p16^{Ink4a}/p19^{Arf}$;$K\text{-}Ras^{v12}$ mice (median survival 45 vs. 26 days; $P < 0.001$). Similarly, the deletion of PTEN in mice with P53-null tumors also had an accelerated tumor onset and progression (*p53*;$p16^{Ink4a}/p19^{Arf}$;$K\text{-}Ras^{v12}$ and *p53;Pten*;$p16^{Ink4a}/p19^{Arf}$;$K\text{-}Ras^{v12}$ gliomas; 28 vs. 20 days, respectively; $P < 0.0001$). These data suggest that activation of the PI3K pathway by PTEN deletion signaling is important in the transformation of cells into high-grade gliomas. We, therefore decided to treat *Pten*;$p16^{Ink4a}/p19^{Arf}$;$K\text{-}Ras^{v12}$ mice daily with 200 mg/kg of ZSTK474, starting 2 days after lentiviral injection. In line with these expectations, ZSTK474 treatment delayed *Pten*;$p16^{Ink4a}/p19^{Arf}$;$K\text{-}Ras^{v12}$;*LucR* tumor onset. However, ZSTK474 was not able to reduce the proliferation rate of these tumors at a more advanced stage (Fig. 6B). Overall, ZSTK474 treatment increased median survival from 26 to 32 days ($P = 0.0002$). Concordantly, PI3K signaling in these tumors was markedly reduced 2 hours after ZSTK474 treatment, while MAPK signaling was unaffected (Fig. 6C). These results suggest that glioma PI3K signaling can be inhibited by ZSTK474 *in vivo*, leading to prolonged survival.

Discussion

This study demonstrates that PI3K inhibitors that are sufficiently brain penetrable can reach levels in glioblastoma that are sufficient for target inhibition and growth delay. Importantly, for ZSTK474, these effects occur at dose levels providing plasma concentrations that are in the range of those achievable in patients (32). However, this work using our spontaneous PTEN-deficient glioblastoma model also shows that inhibition of the PI3K–mTOR pathway alone has very modest activity, most likely due to the fact that, next to the PI3K-mTOR cascade, several other signaling pathways are concomitantly active in glioblastoma.

As manifested by the number of ongoing clinical trials, small-molecule targeted therapies are thought to hold promise for treatment of malignant gliomas. But to be efficacious, these agents need to penetrate the BBB. Besides the more central areas in glioblastoma where the vasculature is leakier, glioblastoma also harbors many tumor cells that have invaded into adjacent normal brain tissue where the BBB is still more or less intact. By using *in vitro* and *in vivo* mouse models, we determined the impact of Abcb1 and Abcg2, two well-established

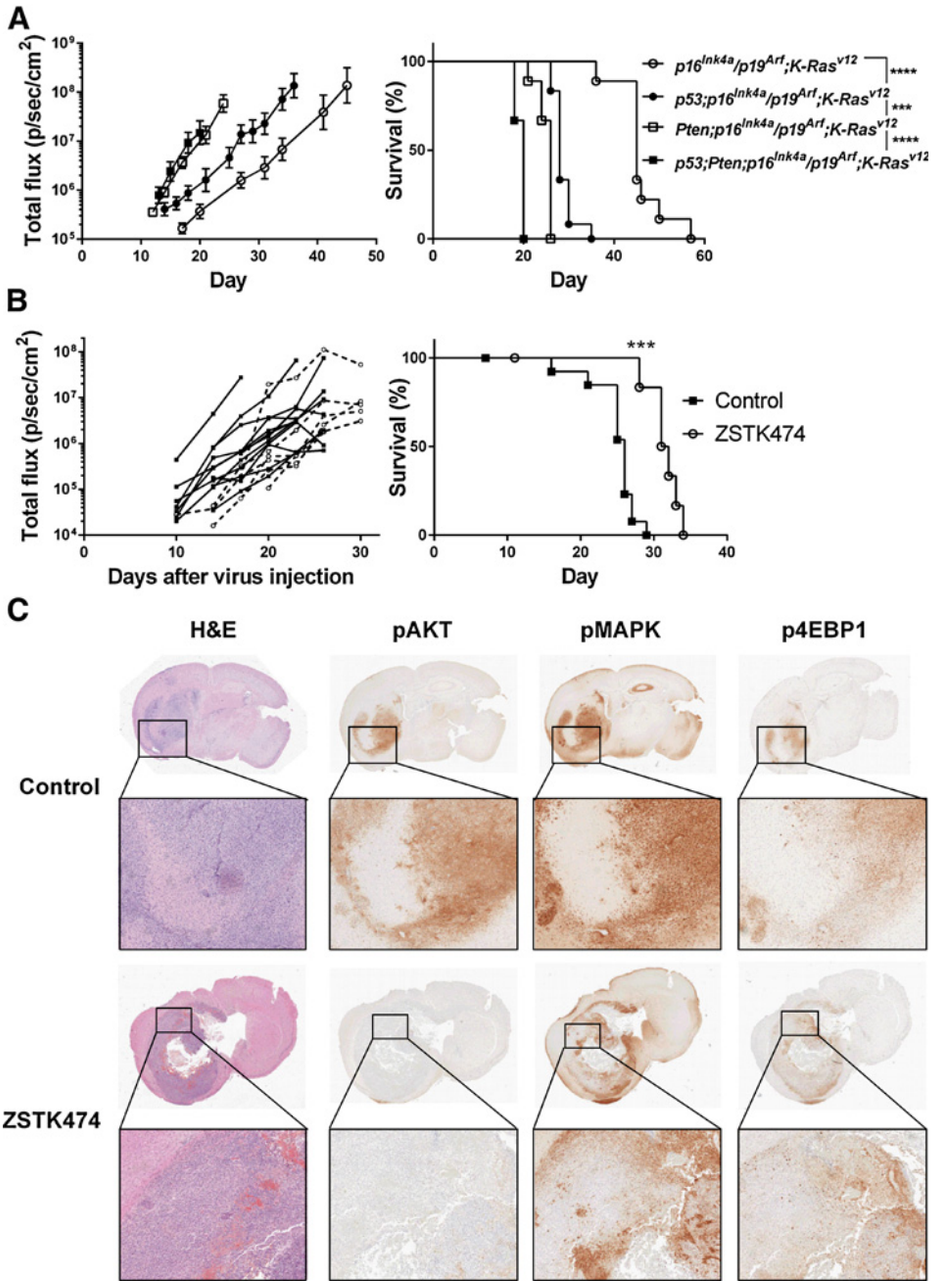

Figure 6.
Efficacy and target inhibition by ZSTK474 in a spontaneous glioblastoma (GBM) mouse model. **A,** Tumor growth and survival of mice spontaneously developing glioblastoma with different genotypes: *p16^{Ink4a}/p19^{Arf};K-Ras^{v12};LucR, Pten;p16^{Ink4a}/p19^{Arf};K-Ras^{v12};LucR, p53;p16^{Ink4a}/p19^{Arf};K-Ras^{v12};LucR* and *p53;Pten;p16^{Ink4a}/p19^{Arf};K-Ras^{v12};LucR*. Data are means ± SD; n = 9–12. **B,** *Pten;p16^{Ink4a}/p19^{Arf};K-Ras^{v12}* conditional mice with spontaneous glioblastoma induced by intracranial injection of lenti-Cre virus received 200 mg/kg every day ZSTK474 or vehicle control starting from day 3 after lentivirus injection. Data are means ± SD; n = 6 and 13 for ZSTK and Control groups, respectively; ***, $P <$ 0.001. **C,** Representative (immuno-) histochemical analyses of coronal brain sections from Control and ZSTK474-treated mice from **B**.

drug efflux transporters expressed at BBB, on the brain penetration of rapamycin, AZD8055, NVP-BEZ235, and ZSTK474. Importantly, for all *in vivo* work with these agents, we have taken the clinically achievable plasma levels into consideration.

Rapamycin is the prototype inhibitor of mTOR and has been tested in clinical trials against glioblastoma without success (33). Because of the Abcb1-mediated brain efflux, the brain concentration of rapamycin (Fig. 1C) remained very low in mice receiving a dose that has previously been used in other preclinical models of cancer (34, 35). In patients, the MTD of daily oral rapamycin is 6 mg/day and results in whole blood levels of about 30 ng/mL (36), thus in the same range as we achieved in WT mice. At this plasma level, however, the brain penetration was insufficient for target inhibition (pS6$^{S235/S236}$) in normal brain tissue of WT mice. Similarly, Mendiburu-Elicabe and colleagues already showed that neither target inhibition nor improved survival was achieved in the U87 xenografts even at a higher dose of 3 mg/kg of rapamycin, while further dose escalation caused severe weight loss (37). In patients undergoing resection of their tumor following rapamycin treatment, the levels in tumor tissue were also in the same range as in the WT mice (38). Rapamycin is not a substrate of Abcg2. The higher level of rapamycin measured in the brain homogenates of Abcg2 mice is a consequence of the high plasma level. The brain-to-plasma ratio

is 0.04, which is close to the fraction of blood that is present in the brain vasculature and that will end up in the brain homogenate (39). Similarly, as shown before for the rapamycin analogue everolimus, the much higher levels of rapamycin in the plasma of the knockout strains is most likely due to the instability of rapamycin in plasma (31) and binding of rapamycin to carboxyl esterase 1c (Ces 1c), which protects rapamycin from degradation. Higher plasma levels in knockout mouse strains were also observed with AZD8055 and NVP-BEZ235, albeit that the effect size was much smaller. This may be due to a similar higher binding to a plasma protein that is more abundant in knockouts. Because of this higher plasma protein binding, the brain-to-plasma ratio will underestimate the brain retention. For rapamycin, the brain-to-blood ratio in *Abcb1a/b* and *Abcg2;Abcb1a/b* knockout mice is about 0.10. The Abcb1/Abcg2 inhibitor elacridar is able to increase the brain level of rapamycin without the increasing the blood level, which results in an increased brain-to-blood ratio from 0.18 to 5.2 in WT versus WT + elacridar animals, respectively. Notably, rapamycin is also strongly retained in brain tissue of *Abcb1a/b* and *Abcg2;Abcb1a/b* knockout mice and causes a profound target inhibition ($pS6^{S235/S236}$) in these strains (Fig. 3D).

Besides insufficient drug exposure, resistance to rapamycin can also be due to the fact that this compound inhibits the formation of the mTORC1 complex, while still causing feedback activation by phosphorylation of AKT at Ser473 by mTORC2 (10, 11). This feedback loop activation of AKT can be negated by using a dual mTORC1/2 inhibitor, like AZD8055, or a PI3K/mTOR inhibitor, like NVP-BEZ235. AZD8055 appeared to be a very good substrate of both Abcb1 and Abcg2, which is in line with previous work showing that AZD8055 (10 mg/kg twice daily) alone was inactive against intracranial glioma (40). Because the plasma levels in mice receiving 10 mg/kg are also considerably higher than can be achieved in patients receiving the MTD (40, 41), we have not further evaluated this compound *in vivo*. Interestingly, the *in vitro* Transwell experiments for NVP-BEZ235 did not show transport by Abcb1 and relatively weak transport by Abcg2. In line with these *in vitro* findings, the impact of Abcg2 on the brain penetration of NVP-BEZ235 was minimal based on the difference between *Abcb1a/b*$^{-/-}$ and *Abcb1a/b;Abcg2*$^{-/-}$ mice. However, Abcb1 significantly decreased the brain concentration and caused incomplete target inhibition in the brains of WT mice. Discordance between *in vitro* Transwell and *in vivo* brain penetration has been observed before (29). In general, the *in vitro* transport model is very effective to identify substrates as shown for rapamycin and AZD8055, but a lack of transport does not always accurately predict the impact of Abcb1 at the BBB. Consequently, *in vivo* studies remain necessary to accurately assess the role of this transporter in drug delivery to the brain. In the case of ZSTK474, the absence of transport by Abcb1 and/or Abcg2 *in vitro* nicely reflected the *in vivo* negligible impact at the BBB. The brain penetration of ZSTK474 was similar between WT and *Abcb1a/b;Abcg2*$^{-/-}$ mice with a brain-to-plasma ratio of 1.5 and profoundly reduced AKT^{S473} phosphorylation even in brains of WT mice. Importantly, this target inhibition occurred at plasma levels that are in the range as those achievable in patients, given that the first-in-human phase I study reported that the plasma level of ZSTK474 in patients who received the MTD (150 mg/kg/day for 21 consecutive days) ranged between 200 and 500 ng/mL (32).

On the basis of these results, we assessed the *in vivo* efficacy of ZSTK474 against orthotopic U87 glioblastoma and included NVP-BEZ235 as a reference, as previously studies have shown that NVP-BEZ235 is active against ectopic (subcutaneous) and orthotopic U87 when given at a daily oral dose of 25 or 45 mg/kg (19, 42). We also found a modest efficacy of NVP-BEZ235 against intracranial U87, even at a lower dose of 10 mg/kg. The plasma concentration in our WT mice was 200 ng/mL in line with the 1,000 ng/mL (peak) and 15 ng/mL (trough) plasma level at a dose of 50 mg/kg as reported by Maira and colleagues (42). Notably, this appears to be considerably lower than the 1,800 ng/mL found in patients as has been presented in a meeting report (43). No other (full) reports on the plasma pharmacokinetics of NVP-BEZ235 have been published, but apparently patients tolerate higher plasma levels than mice, and the efficacy of NVP-BEZ235 will likely be better at higher doses. On the other hand, intracranial U87 gliomas have a very open (leaky) vasculature, which renders the tumor highly accessible for systemically administered drugs. Although it is being used a lot in preclinical research, it is not the most predictive model for clinical efficacy against glioma. Therefore, we decided to test ZSTK474 in one of our spontaneous transgenic glioma models (21). We have used the *Pten;p16*^{Ink4a}*/p19*^{Arf}*;K-Ras*^{v12} spontaneous tumors because PTEN-deficient tumors developed much more rapidly than PTEN-proficient tumors in *p16*^{Ink4a}*/p19*^{Arf}*;K-Ras*^{v12}mice. On the basis of this finding, we expected that inhibiting the PI3K pathway in *Pten;p16*^{Ink4a}*/p19*^{Arf}*;K-Ras*^{v12} mice carrying spontaneous glioblastoma may extend their survival to be comparable as *p16*^{Ink4a}*/p19*^{Arf}*;K-Ras*^{v12} mice. Indeed, we found that treatment with ZSTK474 significantly improved survival and caused inhibition of AKT^{S473} and $pS6^{S235/S236}$ in tumors and surrounding brain. However, the response was much more modest than might have been expected on the basis of the notion that PTEN loss is an important factor driving this model. Glioblastoma is characterized by multiple parallel aberrant signaling pathways (1), and therefore, single-target treatment efficacy will be limited. Combinations with other drugs targeting these other pathways (e.g., MAPK, CDK4/6-Rb) may be necessary. Obviously, these drugs will also need to cross the BBB sufficiently to reach tumor cells in pharmacologically relevant levels. In conclusion, its excellent brain penetration renders ZSTK474 the most promising candidate among the PI3K pathway inhibitors included in this study for future multiple pathway–targeting studies.

Disclosure of Potential Conflicts of Interest

No potential conflicts of interest were disclosed.

Authors' Contributions

Conception and design: M.C. de Gooijer, J.H. Beijnen, O. van Tellingen
Development of methodology: F. Lin, M.C. de Gooijer, R.W. Sparidans, O. van Tellingen
Acquisition of data (provided animals, acquired and managed patients, provided facilities, etc.): F. Lin, M.C. de Gooijer, D. Hanekamp, G. Chandrasekaran, R.W. Sparidans, J.H. Beijnen, O. van Tellingen
Analysis and interpretation of data (e.g., statistical analysis, biostatistics, computational analysis): F. Lin, M.C. de Gooijer, D. Hanekamp, L.C.M. Buil, N. Thota, O. van Tellingen
Writing, review, and/or revision of the manuscript: F. Lin, M.C. de Gooijer, J.H. Beijnen, T. Wurdinger, O. van Tellingen

Administrative, technical, or material support (i.e., reporting or organizing data, constructing databases): L.C.M. Buil, O. van Tellingen
Study supervision: F. Lin, O. van Tellingen
Other (performed some of the *in vitro* and *in vivo* studies): N. Thota

Grant Support

This work has been supported by a grant of the foundation StopHersentumoren.nl (to O. van Tellingen).

The costs of publication of this article were defrayed in part by the payment of page charges. This article must therefore be hereby marked *advertisement* in accordance with 18 U.S.C. Section 1734 solely to indicate this fact.

Received May 19, 2016; revised August 8, 2016; accepted August 17, 2016; published OnlineFirst August 23, 2016.

References

1. Brennan CW, Verhaak RG, McKenna A, Campos B, Noushmehr H, Salama SR, et al. The somatic genomic landscape of glioblastoma. Cell 2013;155:462–77.
2. Parsons DW, Jones S, Zhang X, Lin JC, Leary RJ, Angenendt P, et al. An integrated genomic analysis of human glioblastoma multiforme. Science 2008;321:1807–12.
3. Song MS, Salmena L, Pandolfi PP. The functions and regulation of the PTEN tumour suppressor. Nat Rev Mol Cell Biol 2012;13:283–96.
4. Engelman JA. Targeting PI3K signalling in cancer: opportunities, challenges and limitations. Nat Rev Cancer 2009;9:550–62.
5. LoPiccolo J, Blumenthal GM, Bernstein WB, Dennis PA. Targeting the PI3K/Akt/mTOR pathway: effective combinations and clinical considerations. Drug Resist Updat 2008;11:32–50.
6. Thorpe LM, Yuzugullu H, Zhao JJ. PI3K in cancer: divergent roles of isoforms, modes of activation and therapeutic targeting. Nat Rev Cancer 2015;15:7–24.
7. Kreisl TN, Lassman AB, Mischel PS, Rosen N, Scher HI, Teruya-Feldstein J, et al. A pilot study of everolimus and gefitinib in the treatment of recurrent glioblastoma (GBM). J Neurooncol 2009;92:99–105.
8. Chang SM, Wen P, Cloughesy T, Greenberg H, Schiff D, Conrad C, et al. Phase II study of CCI-779 in patients with recurrent glioblastoma multiforme. Invest New Drugs 2005;23:357–61.
9. Wang X, Yue P, Kim YA, Fu H, Khuri FR, Sun SY. Enhancing mammalian target of rapamycin (mTOR)-targeted cancer therapy by preventing mTOR/raptor inhibition-initiated, mTOR/rictor-independent Akt activation. Cancer Res 2008;68:7409–18.
10. Stoeltzing O, Meric-Bernstam F, Ellis LM. Intracellular signaling in tumor and endothelial cells: the expected and, yet again, the unexpected. Cancer Cell 2006;10:89–91.
11. O'Reilly KE, Rojo F, She QB, Solit D, Mills GB, Smith D, et al. mTOR inhibition induces upstream receptor tyrosine kinase signaling and activates Akt. Cancer Res 2006;66:1500–8.
12. Yilmaz OH, Valdez R, Theisen BK, Guo W, Ferguson DO, Wu H, et al. Pten dependence distinguishes haematopoietic stem cells from leukaemia-initiating cells. Nature 2006;441:475–82.
13. van Tellingen O, Yetkin-Arik B, de Gooijer MC, Wesseling P, Wurdinger T, de Vries HE. Overcoming the blood-brain tumor barrier for effective glioblastoma treatment. Drug Resist Updat 2015;19:1–12.
14. la Fougere C, Suchorska B, Bartenstein P, Kreth FW, Tonn JC. Molecular imaging of gliomas with PET: opportunities and limitations. Neuro Oncol 2011;13:806–19.
15. de Gooijer MC, Zhang P, Thota N, Mayayo-Peralta I, Buil LC, Beijnen JH, et al. P-glycoprotein and breast cancer resistance protein restrict the brain penetration of the CDK4/6 inhibitor palbociclib. Invest New Drugs 2015;33:1012–9.
16. Polli JW, Olson KL, Chism JP, John-Williams LS, Yeager RL, Woodard SM, et al. An unexpected synergist role of P-glycoprotein and breast cancer resistance protein on the central nervous system penetration of the tyrosine kinase inhibitor lapatinib (N-{3-chloro-4-[(3-fluorobenzyl)oxy]phenyl}-6-[5-({[2-(methylsulfonyl)ethyl]amino }methyl)-2-furyl]-4-quinazolinamine; GW572016). Drug Metab Dispos 2009;37:439–42.
17. de Vries NA, Buckle T, Zhao J, Beijnen JH, Schellens JH, van Tellingen O. Restricted brain penetration of the tyrosine kinase inhibitor erlotinib due to the drug transporters P-gp and BCRP. Invest New Drugs 2012;30:443–9.
18. Keen HG, Ricketts SA, Maynard J, Logie A, Odedra R, Shannon AM, et al. Examining changes in [18 F]FDG and [18 F]FLT uptake in U87-MG glioma xenografts as early response biomarkers to treatment with the dual mTOR1/2 inhibitor AZD8055. Mol Imaging Biol 2014;16:421–30.
19. Liu TJ, Koul D, LaFortune T, Tiao N, Shen RJ, Maira SM, et al. NVP-BEZ235, a novel dual phosphatidylinositol 3-kinase/mammalian target of rapamycin inhibitor, elicits multifaceted antitumor activities in human gliomas. Mol Cancer Ther 2009;8:2204–10.
20. Kong D, Dan S, Yamazaki K, Yamori T. Inhibition profiles of phosphatidylinositol 3-kinase inhibitors against PI3K superfamily and human cancer cell line panel JFCR39. Eur J Cancer 2010;46:1111–21.
21. de Vries NA, Bruggeman SW, Hulsman D, de Vries HI, Zevenhoven J, Buckle T, et al. Rapid and robust transgenic high-grade glioma mouse models for therapy intervention studies. Clin Cancer Res 2010;16:3431–41.
22. Lin F, Buil L, Sherris D, Beijnen JH, van Tellingen O. Dual mTORC1 and mTORC2 inhibitor Palomid 529 penetrates the blood-brain barrier without restriction by ABCB1 and ABCG2. Int J Cancer 2013;133:1222–33.
23. Guzman C, Bagga M, Kaur A, Westermarck J, Abankwa D. ColonyArea: an ImageJ plugin to automatically quantify colony formation in clonogenic assays. PLoS One 2014;9:e92444.
24. de Vries NA, Zhao J, Kroon E, Buckle T, Beijnen JH, van Tellingen O. P-glycoprotein and breast cancer resistance protein: two dominant transporters working together in limiting the brain penetration of topotecan. Clin Cancer Res 2007;13:6440–9.
25. Lin F, Chandrasekaran G, de Gooijer MC, Beijnen JH, van Tellingen O. Determination of NVP-BEZ235, a dual PI3K and mTOR inhibitor, in human and mouse plasma and in mouse tissue homogenates by reversed-phase high-performance liquid chromatography with fluorescence detection. J Chromatogr B Analyt Technol Biomed Life Sci 2012;901:9–17.
26. Kemper EM, Leenders W, Kusters B, Lyons S, Buckle T, Heerschap A, et al. Development of luciferase tagged brain tumour models in mice for chemotherapy intervention studies. Eur J Cancer 2006;42:3294–303.
27. Zhang P, de Gooijer MC, Buil LC, Beijnen JH, Li G, van Tellingen O. ABCB1 and ABCG2 restrict the brain penetration of a panel of novel EZH2-Inhibitors. Int J Cancer 2015;137:2007–18.
28. Zhang Y, Huo M, Zhou J, Xie S. PKSolver: An add-in program for pharmacokinetic and pharmacodynamic data analysis in Microsoft Excel. Comput Methods Programs Biomed 2010;99:306–14.
29. Luna-Tortos C, Fedrowitz M, Loscher W. Several major antiepileptic drugs are substrates for human P-glycoprotein. Neuropharmacology 2008;55:1364–75.
30. Ferron GM, Jusko WJ. Species differences in sirolimus stability in humans, rabbits, and rats. Drug Metab Dispos 1998;26:83–4.
31. Tang SC, Sparidans RW, Cheung KL, Fukami T, Durmus S, Wagenaar E, et al. P-glycoprotein, CYP3A, and plasma carboxylesterase determine brain and blood disposition of the mTOR Inhibitor everolimus (Afinitor) in mice. Clin Cancer Res 2014;20:3133–45.
32. Lockhart AC, Olszanski AJ, Allgren RL, Yaguchi S, Cohen SJ, Hilton JF, et al. A first-in-human phase I study of ZSTK474, an oral pan-PI3K inhibitor, in patients with advanced solid malignancies [abstract]. In: Proceedings of the AACR-NCI-EORTC International Conference: Molecular Targets and Cancer Therapeutics; 2013 Oct 19–23; Boston, MA. Philadelphia (PA): AACR. Abstract nr B271. Mol Cancer Ther 2013;12:B271.
33. Reardon DA, Desjardins A, Vredenburgh JJ, Gururangan S, Friedman AH, Herndon JEII, et al. Phase 2 trial of erlotinib plus sirolimus in adults with recurrent glioblastoma. J Neurooncol 2010;96:219–30.
34. Lang SA, Gaumann A, Koehl GE, Seidel U, Bataille F, Klein D, et al. Mammalian target of rapamycin is activated in human gastric cancer and serves as a target for therapy in an experimental model. Int J Cancer 2007;120:1803–10.

35. Thallinger C, Skorjanec S, Soleiman A, Tzaneva S, Griss J, Rous W, et al. Orally administered rapamycin, dacarbazine or both for treatment of human melanoma evaluated in severe combined immunodeficiency mice. Pharmacology 2008;82:233–8.
36. Jimeno A, Rudek MA, Kulesza P, Ma WW, Wheelhouse J, Howard A, et al. Pharmacodynamic-guided modified continuous reassessment method–based, dose-finding study of rapamycin in adult patients with solid tumors. J Clin Oncol 2008;26:4172–9.
37. Mendiburu-Elicabe M, Yin D, Hadaczek P, Zhai Y, Forsayeth J, Bankiewicz KS. Systemic rapamycin alone may not be a treatment option for malignant glioma: evidence from an *in vivo* study. J Neurooncol 2012;108:53–8.
38. Cloughesy TF, Yoshimoto K, Nghiemphu P, Brown K, Dang J, Zhu S, et al. Antitumor activity of rapamycin in a Phase I trial for patients with recurrent PTEN-deficient glioblastoma. PLoS Med 2008;5:e8.
39. Dai H, Marbach P, Lemaire M, Hayes M, Elmquist WF. Distribution of STI-571 to the brain is limited by P-glycoprotein-mediated efflux. J Pharmacol Exp Ther 2003;304:1085–92.
40. Luchman HA, Stechishin OD, Nguyen SA, Lun XQ, Cairncross JG, Weiss S. Dual mTORC1/2 blockade inhibits glioblastoma brain tumor initiating cells *in vitro* and *in vivo* and synergizes with temozolomide to increase orthotopic xenograft survival. Clin Cancer Res 2014;20:5756–67.
41. Naing A, Aghajanian C, Raymond E, Olmos D, Schwartz G, Oelmann E, et al. Safety, tolerability, pharmacokinetics and pharmacodynamics of AZD8055 in advanced solid tumours and lymphoma. Br J Cancer 2012;107:1093–9.
42. Maira SM, Stauffer F, Brueggen J, Furet P, Schnell C, Fritsch C, et al. Identification and characterization of NVP-BEZ235, a new orally available dual phosphatidylinositol 3-kinase/mammalian target of rapamycin inhibitor with potent *in vivo* antitumor activity. Mol Cancer Ther 2008;7:1851–63.
43. Peyton J, Rodon Ahnert J, Burris H, Britten C, Chen L, Tabernero J, et al. A dose-escalation study with the novel formulation of the oral pan-class I PI3K inhibitor BEZ235, solid dispersion system (SDS) sachet, in patients with advanced solid tumors. J Clin Oncol 29: 2011(suppl; abstr 3066).